JOM, Vol. 77, No. 4, 2025
https://doi.org/10.1007/s11837-024-07114-z

TECHNICAL ARTICLE

Advancing Sustainability in Solar-Grade Silicon Production: Enhanced Boron and Phosphorus Removal via Silicon Refining from Al–Si Melt

ABDUL RAHMAN MALLAH ,[1] GUDRUN SAEVARSDOTTIR,[1,2] MATTHIAS HEUER,[3] and HALLDOR G. SVAVARSSON[1,4]

1.—Department of Engineering, Reykjavik University, Menntavegur 1, 102 Reykjavík, Iceland. 2.—Department of Materials Science and Engineering, NTNU, 7491 Trondheim, Norway. 3.—SiQAl UG (haftungsbeschränkt), Bosestraße 40, 12103 Berlin, Germany. 4.—e-mail: halldorsv@ru.is

Solar radiation is a renewable and practically infinite source of energy that creates no greenhouse gas emissions such as CO_2. Photovoltaic devices that turn solar energy directly into electricity are commonly made of high-purity solar-grade silicon, (SoG-Si). The SoG-Si is conventionally produced by a carbothermic reduction of quartz (SiO_2), resulting in roughly 98 wt.% metallurgical grade silicon (MG-Si), which is then further purified into SoG-Si using the Siemens process. The carbothermic step releases a large quantity of CO_2, and conventional purification methods require technically complicated equipment, consume intensive energy, and involve the use and production of highly toxic silane gases. This work has investigated a metallurgical purification method of MG-Si by solidification from aluminum-Si melt. Four purification rounds have been applied to ensure that boron and phosphorus are reduced to 314 ppb_a and 96 ppb_a respectively. A $>$ 99.99 wt.% Si has been obtained, which can be further purified by the directional solidification method, and the purity of Si can be improved to 6N by effectively removing the other elements. The raw material of this process, the MG-Si, was produced by an aluminothermic process without direct CO_2 emissions. Such a process, purification of MG-Si obtained from the aluminothermic reduction of a ferrosilicon slag, by a metallurgical route plus an additional step of directional solidification eliminates the use of highly hazardous silane gases associated with the conventional processes and requires much simpler equipment and lower operational energy, cost, and CO_2 emissions.

INTRODUCTION

Solar energy is an abundant renewable energy source. Earth is irradiated annually by around 1.11×10^9 TWh of solar energy.[1] In comparison, the global electricity production in 2022 was around 18,600 TWh*, whereof only 270 TWh** was obtained by solar cells. Even though solar energy's potential is abundant, some challenges accompany the expansion in the utilization of solar cells.

Commercial solar cells that convert solar radiation into electricity are primarily produced from solar-grade silicon (SoG-Si); furthermore, there are many methods to engineer solar cells to become more independent of the Si purity grade.[2] The conventional process steps to make SoG-Si are carbothermic reduction of quartz (SiO_2) at high temperature, $>$ 1900 °C, to produce metallurgical-grade silicon (MG-Si. $\sim$ 98 wt.%) followed by chemical purification steps, conventionally the Siemens

*Ember's Yearly Electricity Data; Ember's European Electricity Review; Energy Institute Statistical Review of World Energy.

**International Energy Agency (IEA), https://www.iea.org/energy-system/renewables/solar-pv.

(Received August 12, 2024; accepted December 23, 2024; published online January 27, 2025)

or fluidized bed reactor (FBR) processes.[3] Carbothermic reduction requires large amounts of carbon (coke, coal, and woodchips) as a reducing agent, which is turned into CO_2, whereas the further purification of the Si involves using hazardous trichlorosilane ($SiHCl_3$) gas and expensive equipment.[3]

Conventional methods imply environmental impacts represented by releasing significant amounts of CO_2 directly from the process, in addition to indirect emissions due to the electrical energy consumed in the production of MG-Si.[4] Further processing of MG-Si into SoG-Si consumes additional energy and involves hazardous trichlorosilane, which is a flammable, explosive, toxic, and corrosive gas.

The assessed global warming potential (GWP) of the crystalline Si used in solar cells has been reported with a mean of 53 g_{CO_2e}/kWh[5] and can reach up to 560 g_{CO_2e}/kWh[6] based on the carbon footprint of the electricity and the location of the solar cells. These numbers include the carbon footprint of producing MG-Si, which varies from 5 to 20 kg_{CO_2}/kg_{MG-Si}.[4] It is of great interest to develop alternative methods with reduced GHG emissions that eliminate the risks associated with handling trichlorosilane gas.

Several attempts have been made to make SoG-Si directly from MG-Si[7] and bypass the Siemens process. Refining the MG-Si by acid leaching has, for instance, been intensively investigated, and it is usually considered an efficient method to remove metallic contaminations, especially Fe, Al, and Ca.[8,9] The results show that acid leaching alone cannot efficiently remove boron (B) and phosphorus (P) and therefore has to be combined with further process steps.[10] Due to their electrical activities, the levels of B and P are extremely important for SoG-Si. Their high segregation coefficients in solid/liquid Si, 0.8 and 0.35, respectively,[11] make it difficult to remove them during directional solidification of silicon sufficiently.[9,12] Even methods based on electro-chemical refining of Si have not achieved improvement in segregating B since it has thermodynamic properties close to those of Si.[9,13–15] The electrochemical segregation of P is more effective than for B, but the purified Si still does not meet the criteria set for SoG-Si.[13]

The slag oxidation method has been applied by using a slag with a melting point close to that of silicon. Heating the system to a temperature at which slag and silicon are molten leads to oxidation of the impurities[16] and a re-distribution of impurities between both liquid phases. Slags based on $CaO - SiO_2 - CaF_2$, $Al_2O_3 - CaO - MgO - SiO_2$, $CaO - Si - LiF$ were investigated for their potential to remove B.[17–21] The main issue of the slag refining method is that it requires high energy and has different optimal composition ratios for removing B and P.[10]

Purification by vacuum treatments has also been studied, where the refining concept is to melt the Si and remove the impurities by degassing.[10,12] It is found worthwhile to remove P, Zn, and Ca since they have high vapor pressure in molten *Si*.[22–25] As expected with vacuum applications, this method is costly and energy-intensive.

The segregation of impurities during solidification has also been well investigated for different systems like Cu – Si,[26–28] and Al – Si.[11,29,30]

Among several binary systems, the Sn – Si exhibits the lowest B segregation coefficient.[31] However, the Al – Si system has the advantage that the elemental segregation coefficient reduces at lower temperatures,[31–33] which consequently reduces energy consumption. Starting from the work of Dawless et al.,[34] the purification of Si using Al-Si melts has been well studied because of its promising low energy consumption,[35] the potential reduction of the investment and operational costs, and easy implementation. Moreover, the segregation during solidification of Si from molten Al-Si can reduce the percentage of both B and P to < 1 ppm.[36,37] Adding Ti to the solution leads to the formation of TiB_2 particles, which removes the dissolved B from the molten Al-alloy.[32,38]

Even though the reported concentrations of the B and P after metallurgical purification in the literature are relatively low, the material feedstock specifications for photovoltaic applications require lower contaminations at a few hundred ppb or even lower values. The metallurgical methods are always followed by a directional solidification step to remove the impurities. However, and in contrast to most of the elements, the directional solidification process cannot effectively reduce the B and P amount since they have a high segregation coefficient. Hence, the B and P contaminations in the MG-Si must be treated during the metallurgical purification method.

This work has implemented a refining methodology based on the segregation by solidification of MG-Si in Al-Si melt. The MG-Si has been processed through four consecutive alloying rounds with Al. The process includes heating the system to its melting point and then slowly cooling to just above the eutectic temperature to allow crystallization of the Si while the impurities are segregated and confined in the liquid Al-Si phase. The four rounds of Si refining are designated to ensure that concentrations of B and P have fallen to the accepted limits of the photovoltaic applications (only a few hundred ppb). Recycling of the Al within the process has been considered by reusing the Al of high-purity rounds in the lower-purity rounds.

Notably, the raw material of the process, MG-Si, was obtained using aluminothermic reduction method by using a secondary aluminum (aluminum dross, end-of-life scrap, etc.) as a reducing agent and resulted in negligible direct CO_2 emissions.[39–41] The MG-Si obtained by the aluminothermic route is rich in calcium. However, the metallurgical purification method presented in this work reveals very effective removal of calcium.

This study is an experimental trial to investigate an alternative route for the SoG-Si industry considering enhancing sustainability, simplifying the process, and reducing energy consumption. A thermodynamic analysis study is also presented in this work to evaluate the minimum theoretical energy and material needs of the presented process for different scenarios.

EXPERIMENTAL PROCEDURE

Purification from Al-Si Melt

Silicon melts at 1410 °C and Al at 660 °C. Silicon can be dissolved in molten Al to a certain extent, forming a binary Al-Si alloy with a distinct eutectic temperature of 577 °C. A phase diagram of the binary system is shown in Fig. 1. At 1050 °C, the Al can dissolve an equal amount of Si (50/50 mass ratio). During heating, the impurities in the MG-Si mix with the melt. Upon cooling, crystallized Si precipitates, leaving most of the impurities in the liquid phase (molten Al-Si phase). When the system is cooled to 650 °C or slightly below, most of the Si in the system is precipitated and Al-Si remains in a liquid form together with the impurities originating from the MG-Si. The purified and crystallized Si then needs to be separated from the melt.

Understanding this purification process requires knowledge of the segregation coefficient of impurities between solid and liquid phases. The segregation coefficient, denoted as k_e and theoretically defined in Eq. 1, represents the remaining mole fraction ratio of the impurity in the solid silicon $\chi_{e-\mathrm{Si}}$ to liquid phase $\chi_{e-\mathrm{liquid}}$.

$$k_e = \frac{\chi_{e-\mathrm{Solid}}}{\chi_{e-\mathrm{liquid}}} \quad (1)$$

Yoshikawa et al.[11] depicted that the segregation coefficient reduces at lower temperatures, i.e., more efficient impurity removal can be achieved at lower temperatures. Hence, the solidification of Si from the Al/Si solvent helps to remove the impurities since the solidification temperature drops from 1410 °C for the Si to < 1100 °C for the Al/Si (50%/50%) composite. The main advantage of the solidification from molten Al/Si is that it significantly reduces the segregation coefficients of both elements from 0.8 and 0.35, respectively, into < 0.2 at temperatures < 1000 °C (Fig. 2).

Directional solidification is an efficient process of removing the impurities from silicon and upgrading the material to comply with the requirements of SoG-Si. However, both B and P have high segregation coefficients at the directional solidification temperature (1414 °C) in solid/liquid Si (0.8 and 0.35, respectively) compared to a coefficient below 10^{-3} for other elements.[10]

Therefore, there is only a limited reduction of B and P during directional solidification, and the crystallization of Si from Al/Si-melt has clear advantages. Hence, four rounds of purification in the molten Al/Si were conducted in this work to reduce the B and P contaminations to a level of a few hundred ppb, which fulfills the requirements of SoG-Si. It is apparent that more rounds will give a marginal reduction of the contamination at a high cost in terms of energy and material as will be depicted in the evaluation of energy consumption (Section "Evaluation of the Energy Consumption").

For the two last purification steps (the third and the fourth), Al with very low concentrations of B and P (< 1 ppm) was used whereas master alloys resulting from steps 3 and 4 (resulted from a previous experiment) were used in steps 1 and 2 of the next batch (Fig. 3).

The MG-Si used in this process was obtained by a reduction of SiO_2 in aluminothermic reaction by the SisAl Pilot partner, Elkem, Norway. A quantitative analysis of the Mg-Si is presented in the results section.

Three batches of 1.6 kg MG-Si (4.8 kg in total) were gradually added to 5.2 kg of molten Al at 800 °C, 900 °C, and 1000 °C, respectively, to facilitate rapid dissolution of Si. The mixture was then

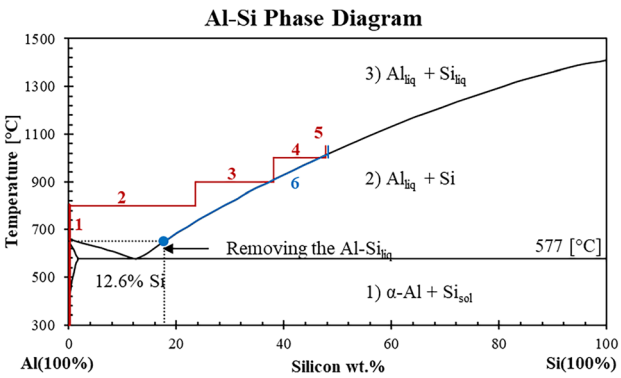

Fig. 1. Phase diagram of the Al-Si system. (Original artwork, data source:[42] replotted along with details of the purification process.) Schematic expression of the purification steps taken (refer to Table I).

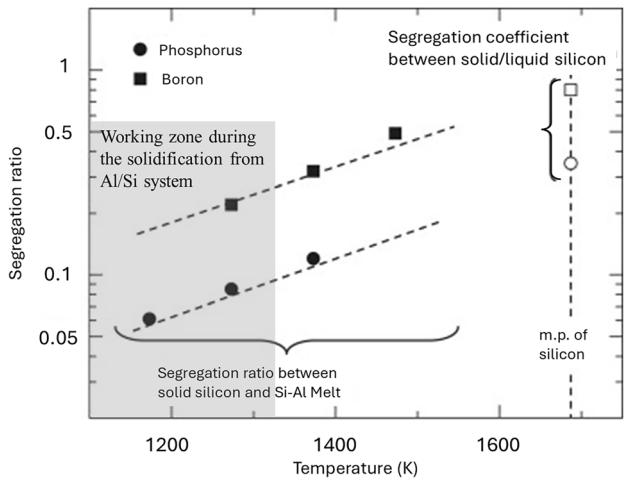

Fig. 2. Segregation coefficient of P and B elements in the solid Si and liquid Al/Si. Reprinted with permission from Ref. 11.

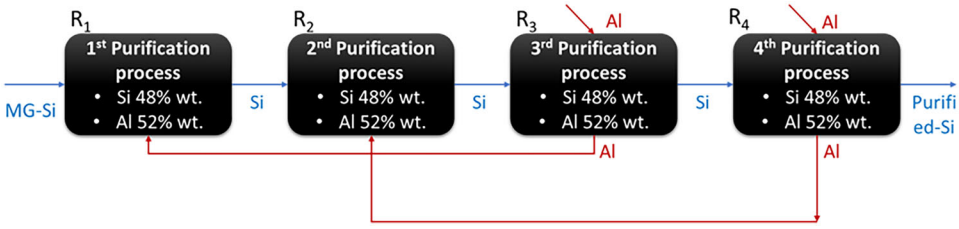

Fig. 3. Schematic expression of the four steps taken in the purification process.

heated to 1050 °C and held at that temperature for 2 h to ensure a homogeneous heat distribution and a complete dissolution of the Si. Subsequently, the alloy was cooled at 25 °C/h from 1050 °C to 650 °C (the total cooling time is 16 h). Slow cooling is important for the Si to crystalize with minimal inclusion of impurities.

There are two reasons to design a process with a low cooling rate: The first is to minimize the amount of aluminum trapped within the crystallized silicon. The high cooling rate causes the fast growth of relatively large Si crystals, which trap Al at different locations inside the bulk Si crystals. The trapped Al is difficult to remove even with the acid washing step applied later since the trapped Al is not exposed to the acidic solution. Even though at a low cooling rate, the chemical analysis of final Si crystals (after acid washing) always shows at least 60 ppm Al concentration. Increasing the cooling rate leads to an increment in the amount of remaining Al, which creates further issues in the directional solidification step. The second reason is related to the purification mechanism and the kinematics of impurities' migration from the solid phase into the liquid phase. The Si crystals that are newly formed contain impurities. The purification from Al-Si solution effectively happens during the recrystallization step. At a relatively low temperature, the segregation of elements with similar thermodynamic properties of Si is more efficient. Hence, giving enough time for silicon crystals to grow and be in direct contact with the liquid helps to segregate B and P beside the other elements.

At 650 °C, most of the Si in the system is solidified, so the remaining Al melt is removed. The process was repeated another three times following the quantity of the materials listed in Table I.

The Al master alloy obtained from every purification round retains around 17 wt.% of Si. The parameters of the first round of purification are available in Table I.

The Si crystals obtained from the melt after four purification rounds are further treated with HCl acid to remove the solidified Al covering the Si crystals (leaching). The leaching was conducted by adding 20 mL of 15 wt.% HCl to each 1 g of the Si alloy. The equation below describes the chemical reaction taking place in the leaching:

$$2Al + 6HCl \rightarrow 2AlCl_3 + 3H_2 \quad (2)$$

Material Characterization

After leaching with HCl and washing and drying the resulting Si particles and flakes, the Si crystals were analyzed quantitatively and qualitatively.

Scanning electron microscopy (SEM, Zeiss Supra 25 Field Emission) was used to examine the Si particles and selectively verify the structure quality at the micro-scale. Energy dispersion x-ray spectroscopy (EDS, Oxford Instruments, AZtec Advanced software) was used to perform a chemical analysis of the main compounds.

X-ray diffraction (XRD, Panalytical Empyrean) was used to investigate the phases using copper K-alpha radiation. The system was equipped with a Bragg-Brentano HD mirror on the incident side and a divergence slit plus a PIXcel3D detector to measure the diffracted beam.

A qualitative and quantitative chemical analysis was performed by inductively coupled plasma optical emission spectroscopy (ICP-OES, Ametek Spectro Arcos FHS12) and ICP mass spectrometry (ICP-MS, Agilent Technologies 7800).

Assessment for Directional Solidification Process

Silicon, purified by metallurgical methods, still contains traces of residual impurity elements. After that, the directional solidification (DS) step is an important additional process in which the Si is melted and then slowly directionally cooled (usually vertically) at a rate that usually ranges between 5 μm/s and 110 μm/s.[38] Inclusions can accumulate at certain regions on the top and/or bottom. In addition, most of the impurities are segregated at this step at a rate that depends on their segregation coefficient. At the end of the directional solidification, the top and bottom layers, containing the residual impurities, are cut off.[10]

Apart from B and P, most other elements can be significantly reduced by DS. The concentration of impurities after the DS ($C_{e,DS}$, Atom/cm^3) is related

Table I. Technical details for the first round of purification by the solidification in the Si/Al system

Step	Process	Weight (kg)	Temperature (°C)	Dwell time (h)
1	Heating of the Al	5.2	800	0.5
2	Adding MG-Si and mixing	1.6	800	0.5
3	Adding MG-Si and mixing	1.6	900	0.5
4	Adding MG-Si and mixing	1.6	1000	–
5	Holding the system temperature	1050	2	
6	Cooling with a rate of 25 °C/h	650	–	

Table II. Summary of the ICP analysis of the purified Si and the expected purity of the silicon after one round of directional solidification (DS) at 1414 °C

	Element	MG-Si starting material (Elkem) (ppb_a)	Purified Si (ppb_a)	1st DS /1414 °C (ppb_a) (estimation)*
Acceptors	B	37,697	314	284
	Al	4,881,358	68,150	274
Donors	P	7359	96	52
	As	3814	6	~ 0
	Sb	28,473	31	~ 0
Transition metals and post-transition metals	Ti	430,597	77	~ 0
	Cr	71,303	4	~ 0
	Fe	4,139,381	274	~ 0
	Ni	44,069	7	~ 0
	Cu	24,154	~ 0	~ 0
	Zn	~ 0	~ 0	~ 0
	Mo	3000	26	~ 0
Alkali and earth alkali metals	Na	42,950	37	~ 0
	K	~ 0	36	~ 0
	Ca	9,017,961	355	~ 0
Other elements	Ni	44,070	7	~ 0
	Mn	215,214	5	~ 0
	V	69,329	6	~ 0
	W	6850	8	~ 0
	Mg	141,099	59	~ 0
Purity of the Si	Si	~ 98.1%	~ 99.99%(~ 4N)	~ 99.9999%(~ 6N)

to the initial concentration of the element e ($C_{e,i}$, $Atom/cm^3$) and the segregation coefficient of the element, k_e, in the liquid silicon at 1414 °C, considering the factors of top and bottom cut after solidification (fs_T, fs_B):[43,44]

$$C_{e,DS} = C_{e,i} \times \left(\frac{(1 - fs_B)^{k_e} - (1 - fs_T)^{k_e}}{(fs_T - fs_B)} \right) \quad (3)$$

A list of elements and their amount obtained by the ICP-MS and ICP-OES is given in Table II. Based on their concentration and segregation coefficient in the molten Si, the material from the leaching was assessed to predict the purity of the Si that could be expected after the DS process.

RESULTS AND DISCUSSION

Purification of MG-Si

MG-Si is the feedstock of the current process, and its analysis is briefly depicted in Fig. 4. The EDX analysis of arbitrary sites reveals the domination of Si with the existence of other metallic atoms like Fe, Cu, and Al. However, the XRD inspection shows only the Si crystal diffraction pattern; a more detailed chemical analysis is shown in Table II. The purification of the MG-Si was carried out as per the process described before. When the temperature reached 650 °C, most of the Si had precipitated as small crystallites and formed a network of fragile flakes. The molten Al phase was removed at 650 °C,

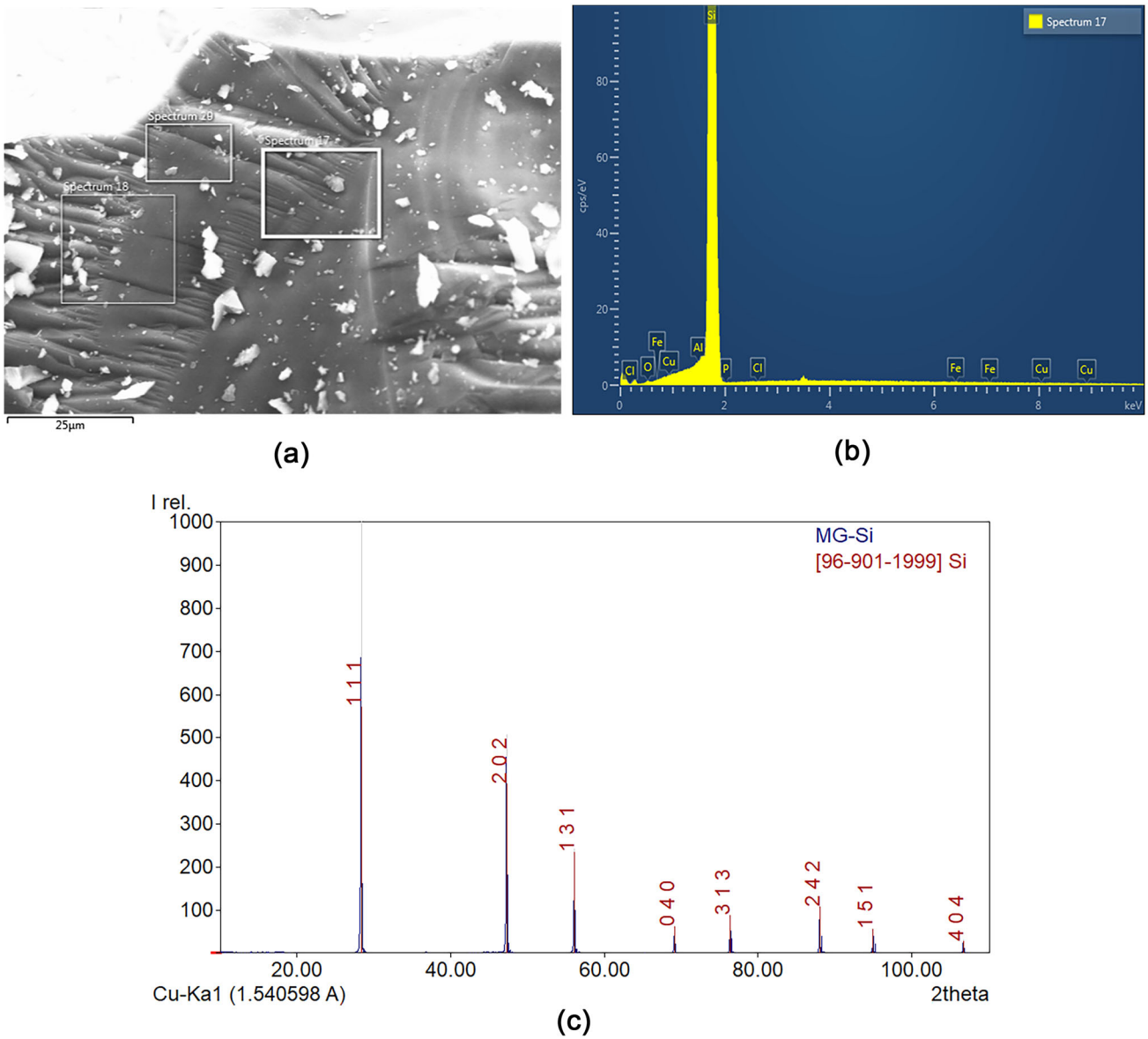

Fig. 4. MG-Si characterization: (a) SEM image, (b) EDX analysis, and (c) XRD diffraction pattern.

after which the solidified Si was gathered and processed again by adding the collected Si into another batch of melted Al. The melting process was repeated four times to reduce the impurities levels at which further purification by directional solidification is expected to provide SoG-Si.

The MG-Si precursor used, in the form of metallic chunks, is shown in Fig. 5a. Figure 5b illustrates a cross-section of the Al-Si alloy in the crucible after complete solidification of the system. Aluminum appears in a lighter gray, whereas the darker flakes and stripes represent Si crystals. A network of Si flakes after leaching is shown in Fig. 5c. The flakes' surfaces are mirror-shiny and come in different sizes ranging from sub-millimeters to several millimeters. The flakes are fragile and structurally weakly connected, so they can be easily detached and broken by light mechanical force during the chemical leaching.

Several trials were carried out to optimize the leaching process. It has been found that applying external heating gives worse results. The HCl reaction with Al is highly exothermic, and external heating leads to the evaporation of the liquid and the formation of Al_2O_3 (alumina). Hence, leaching with HCl has been carried out with the absence of external heating in contrast to the previous study by Santos[45] where it was reported that acid leaching at elevated temperatures helps to reduce the contaminations.

The formation of alumina was the main issue encountered during the leaching process. It is quite difficult to remove the alumina particles once they are formed and adhere to the Si particles. Hence,

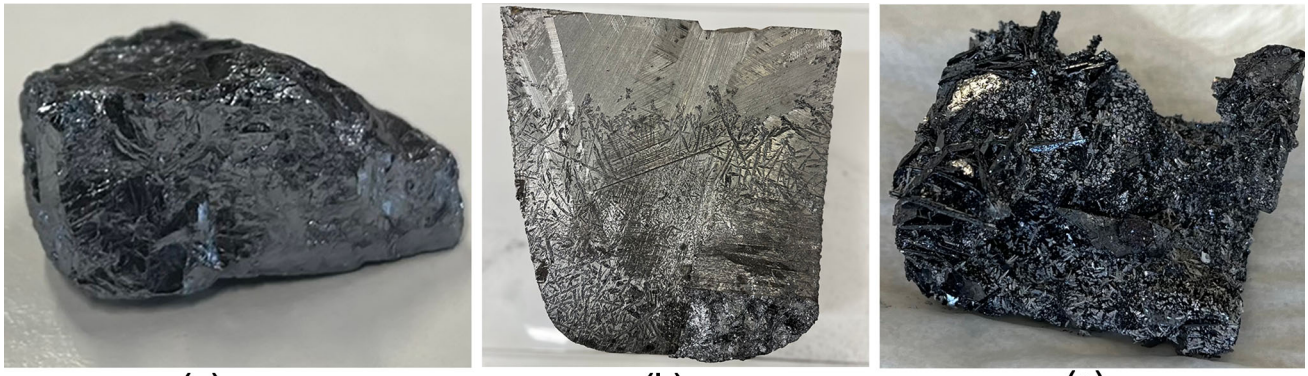

Fig. 5. Photographs of solidified phases. (a) MG-Si precursor from Elkem, (b) cross-section of the Al-Si alloy after four rounds of purification and solidification, and (c) network of Si-flakes after removing the Al by leaching.

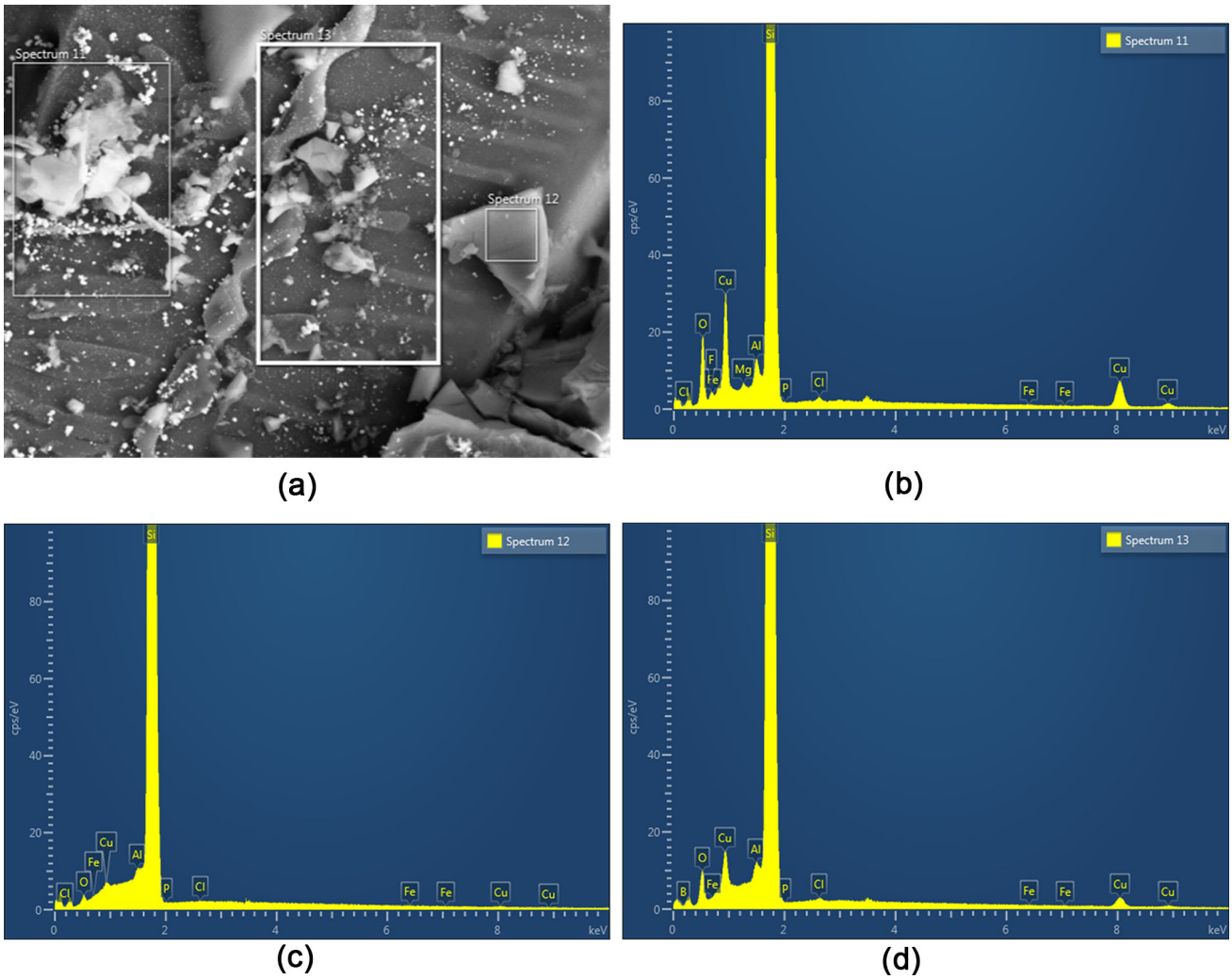

Fig. 6. Analysis of Si particles leached with HCl and additional heating: (a) SEM; (b–d) EDX analysis at different sites.

working on preventive actions during the leaching reaction is crucial to maintain the process as simple as possible. The SEM and EDX screening shows that acid leaching associated with heating results in less efficiency in removing the elements besides forming metal oxides. An example of material analysis after leaching with heat is depicted in Fig. 6; similar results are always observed for a reaction with additional heat.

The material leaching with HCl removes the remaining aluminum that covers the silicon flakes. Therefore, it is a washing process rather than a purification step for removing the impurities. During the leaching process, the flakes break into smaller pieces because of the dissolution of trapped aluminum within the flakes. The remaining aluminum contains impurities from the MG-Si. The efficiency of the leaching by HCl is high in removing most of the Al stuck on the outer surfaces of silicon flakes, but the trapped Al inside the flakes and not exposed directly to the acid remains in the Si particles. The ICP analysis shows that the aluminum concentration after the acid leaching is at least 60 ppm.

The best leaching practice was found when running the reaction at a low concentration of HCl, starting from 5 wt.%. After 2–3 h of reaction, the flakes usually break into smaller flakes and finer particles. At this stage, the acid concentration could be increased to 10 wt.% When most of the Si particles had become very small, the HCl concentration was raised to 15 wt.%. By following this practice, the formation of alumina was reduced.

A by-product of the leaching, the aqueous solution $AlCl_3$ has value as a chemical in several industries; for instance, it can be used as a flocculant to treat wastewater besides its applications in the rubber and paint industries. The other by-product, hydrogen gas, also has value in the energy industry. Therefore, the by-products of the leaching process can be used, and almost no waste is generated. At the end of the reaction, the leached Si particles are separated by filtering the solution.

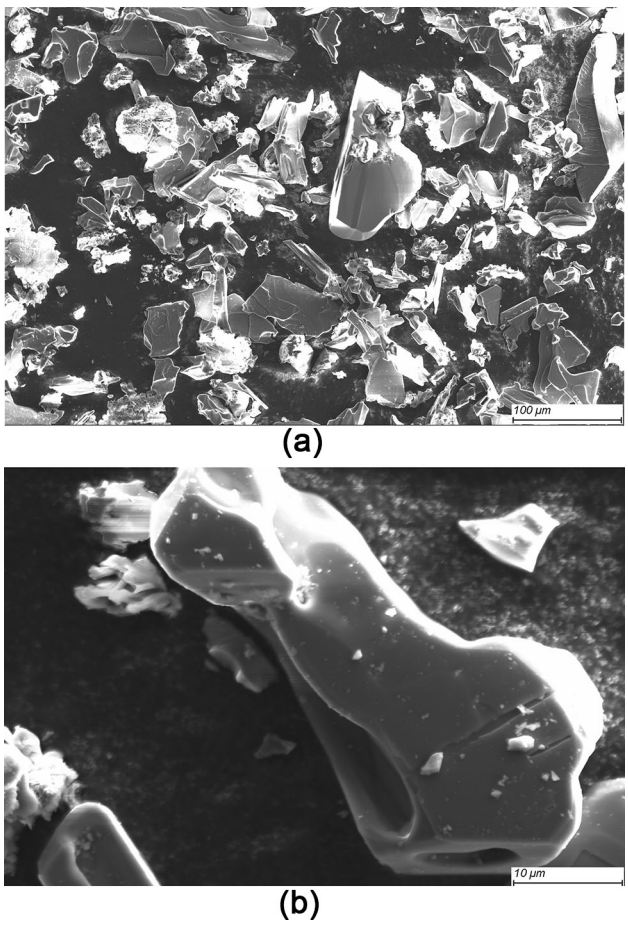

Fig. 7. SEM micrographs of purified silicon at different sites and different magnifications.

Material Characterization

An SEM image of typical Si-crystallites obtained after purification and leaching is shown in Fig. 7 in two different magnifications. The crystalline nature of the solid particles is apparent as it is characterized by sharp edges and smooth shiny surfaces.

EDX method was applied to analyze the elemental composite of selected zones within the samples. Even though a higher accuracy inspection method of ICP was also followed, the EDX method can visualize the elemental distribution in the samples and reveal the existence of some elements like carbon and oxygen that the ICP cannot measure. EDX analysis exhibited that most of the particles consist of Si with a trace of Al oxide as depicted in Fig. 8. EDS analysis of an arbitrary site 1 reveals that 99.9% of the area is Si with a negligible amount of metal oxide. The small carbon peak seen is probably related to the carbon tape the sample was attached to. Two small particles in the analyzed site are composed of Al, O, and Si. These two particles are probably a mixture of Al-oxide beside Si and Si-oxide. The accurate quantitative elemental analysis will be presented when discussing the ICP results.

Another example of the EDX results for arbitrary site 2 is shown in Fig. 9, where only Si was detected. The measured energy for oxygen at site 2 is remarkably low and can be neglected since the dispersion energy of oxygen is below 0.5 keV. The observation of site 2 indicates that Si is dominant on the surface, which reflects the purity of the Si particles as purified by the metallurgical method.

The EDX inspection was made for several areas in the sample with similar results in all cases. Notably, the presence of Al-oxide particles indicates that the leaching process should be further improved; it is also noted that heating the solution during the acid leaching led to an increased number of Al_2O_3 particles. Additionally, the more Al_2O_3 particles observed with the SEM/EDX inspection, the greater the concentration of other contaminations of the respective sample when analyzed by ICP. Apparently, there is a correlation between the increase of Al_2O_3 and the increasing contamination of most of the other elements, which indicates that the Al_2O_3 particles incorporate other impurities.

To quantitatively investigate the structure of the particles and obtain the phases that existed in the purified material, XRD measurements were performed. The measurement was taken within the range $2\theta = 10°–120°$ with a scanning period of

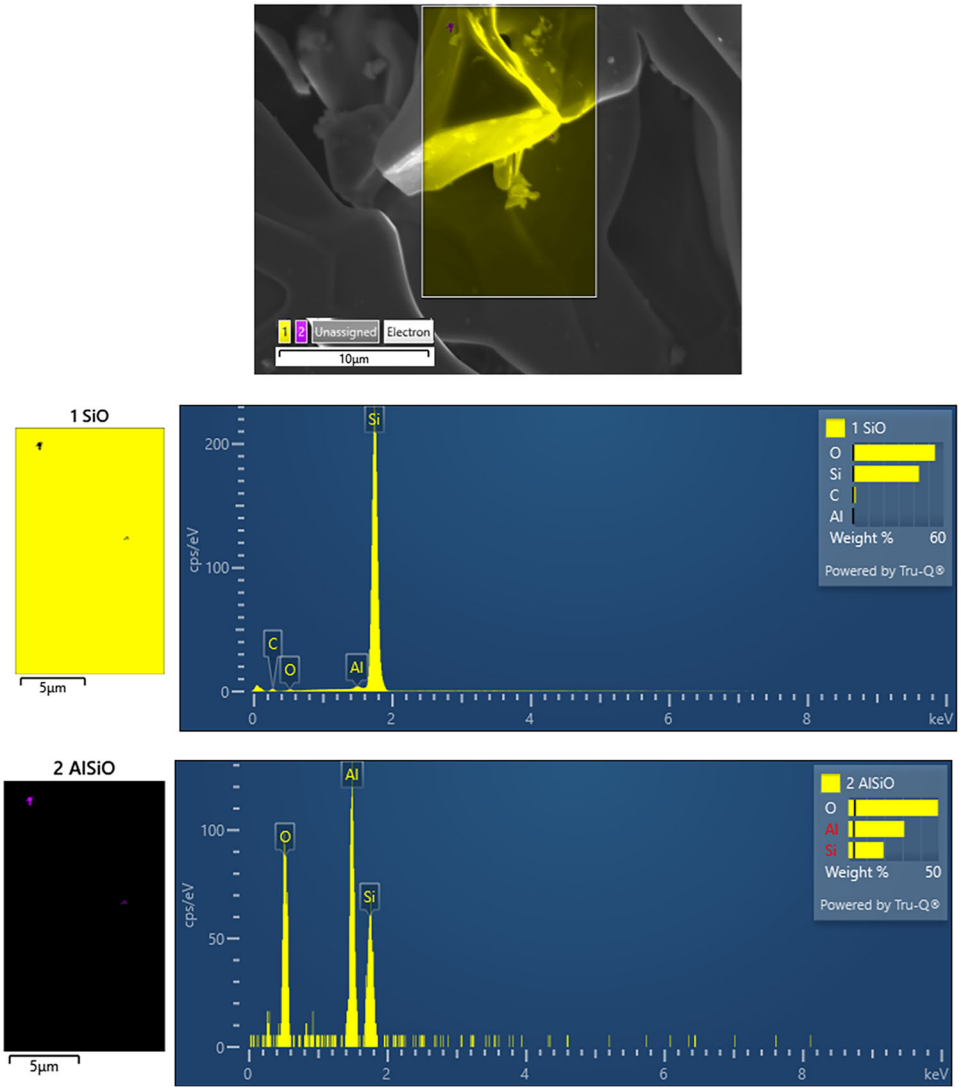

Fig. 8. EDX analysis for the chemical composition of arbitrary site 1 of the purified material.

20 min. The XRD pattern of purified particles perfectly matches with crystalline Si for all eight diffraction peaks of the main crystallographic phase (Fig. 10). Additionally, small amounts of other phases have been detected, but could not be identified.

For further quantitative chemical analysis of the purified silicon, and to precisely obtain the impurity concentrations of the powder, samples were measured by ICP-OES and ICP-MS; the results are shown in Table II. The purified Si has a low level of contamination for all the inspected elements except for Al. The most significant result is the low content of B and P, which indicates an efficient purification process since those two elements are difficult to remove by other methods. A purity of ~ 99.993% (4N3) Si was achieved. The expected purity after adding DS to the purified Si-flakes was calculated, based on the segregation coefficients of the elements in Si at 1414 °C.[46]

Notably, except for Al, B, and P, all other elements could fall in the highest purity class for SoG-Si. B and P concentrations are expected to be reduced to residual levels below 300 ppb_a after the first directional solidification due to their high segregation coefficient. With 68 ppm_a, the Al concentration in the purified Si is still high. The result of aluminum is expected since there will always be Al trapped inside the Si flakes and particles during the crystals' growth inside the Al-Si melt. However, Al can be efficiently removed during the directional solidification of the purified silicon, which has to be made anyway to convert the Si into chunks, which is the preferred shape for customers of SoG-silicon.

The purity level is estimated to increase to 6N as it feeds into directional solidification. The MG-Si produced by the SisAl process contains a significant amount of Ca, around 9000 ppm. However, it is still under control in further purification for preparing the SoG-Si since a significant amount of it is just

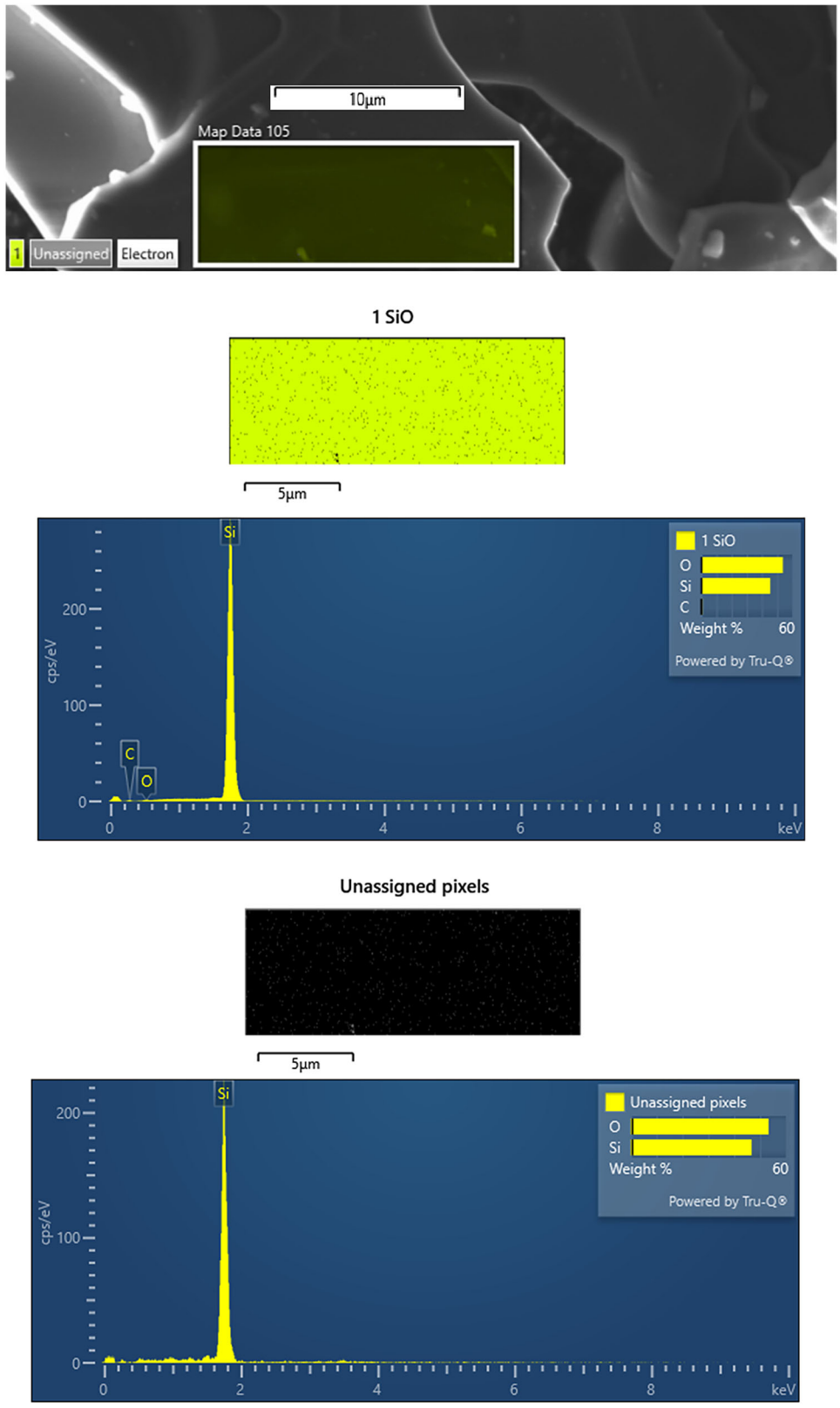

Fig. 9. EDX analysis for the chemical composition of an arbitrary site 2 of the purified material.

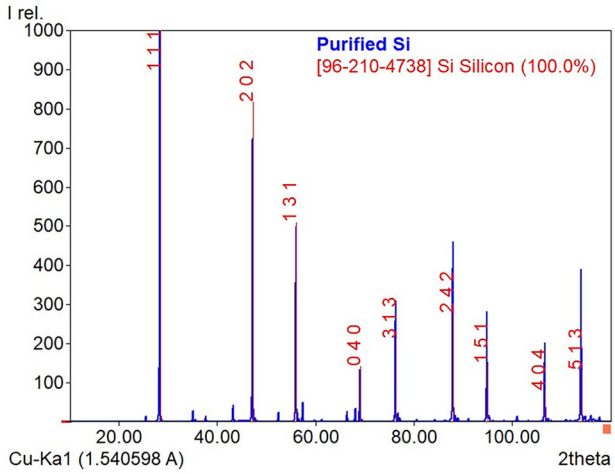

Fig. 10. XRD diffraction pattern of purified and leached Si (blue color) and a Si reference material (96-210-4738) (red color) (Color figure online).

oxidized at the surface of the Al melt. Furthermore, the segregation coefficient of Ca is relatively low in liquid Al, so the directional solidification is supposedly capable of removing most of the remaining Ca.

During the purification of the Si in the Al melt, the Al melt is removed at 650 °C. Around 15–20% of the Si is still dissolved at this temperature and is left in the Al melt (refer to Fig. 1). When repeating the purification for another three rounds, around 70-75% of the original Si has been left in the melt. This loss is reduced by reusing Al obtained from the higher purity steps (3rd and 4th) at the lower purity steps (1st and 2nd) as shown schematically in Fig. 3. Furthermore, it must be noted that losing silicon into the melt does not necessarily mean economic losses for such process in a production. The spent melt can be cast into sows and then sold as a master alloy for making Si-containing Al alloy products.

Evaluation of the Energy Consumption

It is necessary to evaluate the energy consumption to verify the extent to which the metallurgical purification method, presented in this study, could reduce the energy required to reach the purity of SoG-Si. Also, it helps to quantify the material flow in the process for different scenarios of recycling for the Al alloys.

The evaluation presented here includes both processes: the purification from the molten Al/Si system and the directional solidification. The energy evaluation is applied for the energy required to heat the Si and the Al to the desired temperature. However, the losses due to heating of the other external parts like crucibles and furnace/s are not considered. Hence, the estimate gives an idealized limit representing the process's inherent consumption, which cannot be further reduced by minimizing losses. Also, the other processes including acid leaching and material transport, material crash,

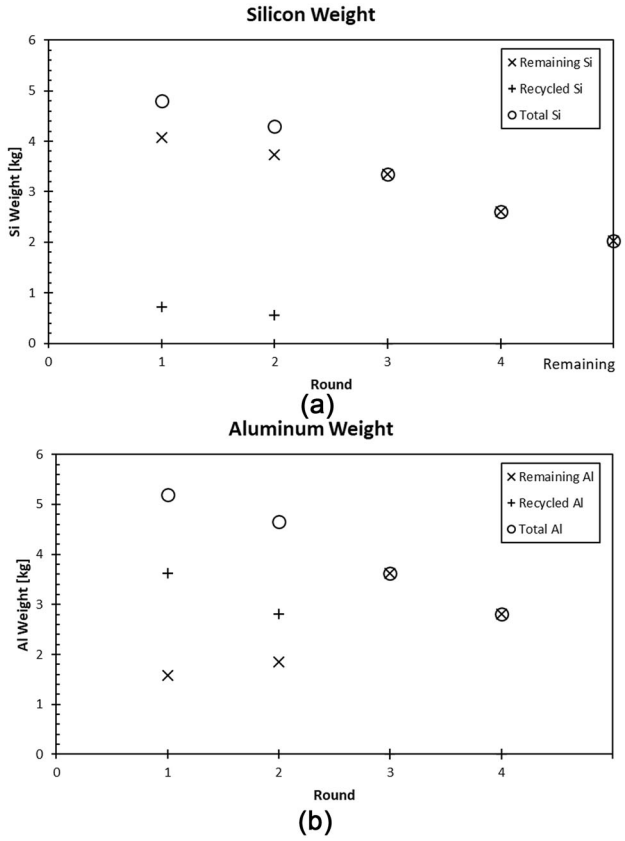

Fig. 11. Mass balance for a process according to Scenario 3: (a) silicon weight and (b) aluminum weight.

etc., were ignored. Furnaces are assumed to be perfectly insulated so the normal heat loss has not been considered. In addition, Si recovery after each purification round is assumed to match the theoretical amount indicated by the Al/Si phase diagram at 650 °C.

The required energy to heat the Al from T_1 to T_2 is described by:

$$Q_{h-Al} = m \cdot cp \cdot (T_2 - T_1) + Q_{\mathrm{Al-latent}} \qquad (4)$$

where m and cp are the mass and the specific heat of Al, and $Q_{\mathrm{Al-latent}}$ is the latent heat of melting for aluminum, 405 kJ/kg. A similar formula is used for Si except that the enthalpy of fusion $\Delta H^F_{\mathrm{Si-Al}}$ is used instead of the latent heat of melting, and the required heat is:

$$Q_{h-Si} = m \cdot cp \cdot (T_2 - T_1) + \Delta H^F_{\mathrm{Si-Al}} \qquad (5)$$

The enthalpy of fusion is a function of the percentage of dissolved silicon χ^l_{Si} in a liquid phase and to an experimental factor (a):[47]

$$\Delta H^F_{\mathrm{Si-Al}} = a \cdot \left(1 - \chi^l_{\mathrm{Si}}\right)^2 \qquad (6)$$

a was found equal to − 348.57 (kJ/kg),[47,48] and the corresponding averaged enthalpy for the temperature range 577 ºC to 1100 ºC is around − 174.84 (kJ/kg).

Four case scenarios were studied based on Al recycling:

1. Without Al recycling (Scenario 1).
2. Recycled Al alloy from round 4 used in round 1 (Scenario 2).
3. Recycled Al alloy from rounds 3 and 4 is used in rounds 1 and 2 (Scenario 3) (used in this work).
4. Recycled Al alloy from rounds 2, 3, and 4 is used in rounds 1, 2, and 3 (Scenario 4).

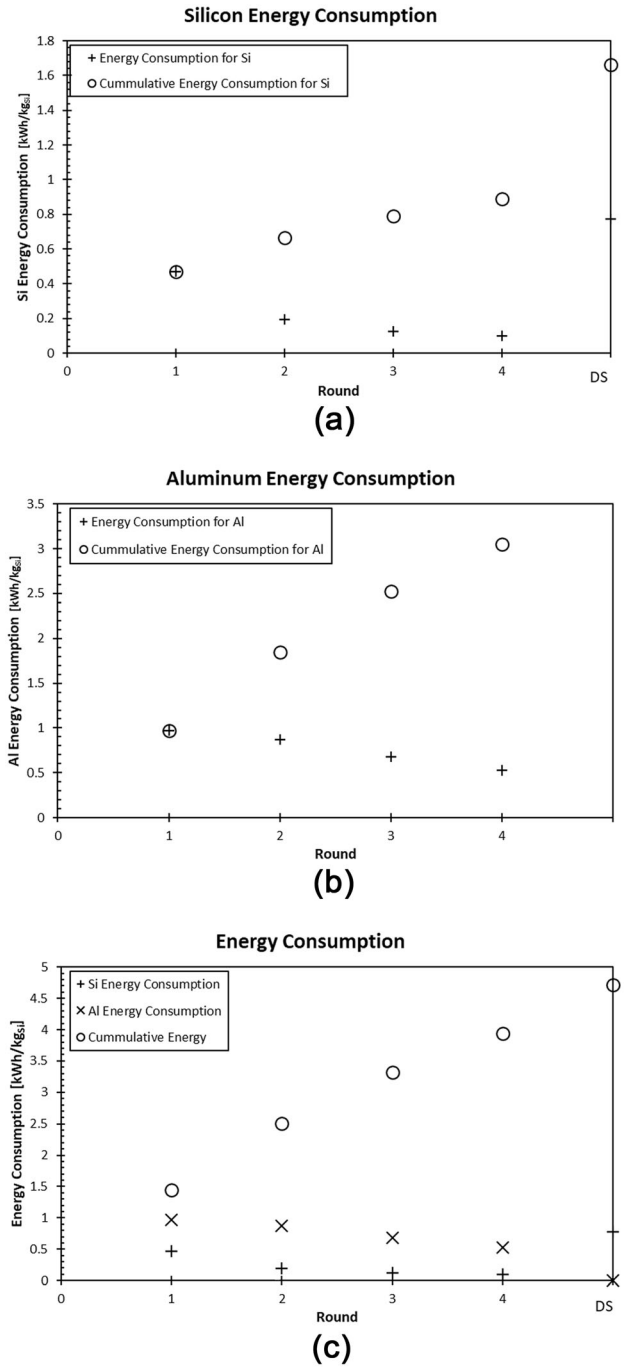

Fig. 12. Energy consumption breakdown for a process according to Scenario 3: (a) silicon, (b) aluminum, and (c) total energy consumption.

The recycled Al contains dissolved Si. Hence, the more recycled Al is involved in the process, the more the Si recovery rate can be raised and, consequently, less energy is required per mass unit of SoG-Si.

Every round has 48% Si and 52% Al. The recycled Al and the remaining Si are assumed to be added at room temperature (25 °C), so the diffusion enthalpy of Si was also considered for the recovered silicon. Figure 11 reveals the mass balance of Si and Al for a process according to Scenario 3, where recycled Al alloy is used in rounds 1 and 2. Recycling of the Al alloy ensures returning around 0.724 kg Si to the first round and 0.56 kg Si to the second round. The returned Si forms approximately 63% of the remaining Si after four purification rounds. A similar figure for Al recycled in the system, using recycled alloy in two rounds, leads to using 6.43 kg of Al, which forms approximately 39% of the total Al used in the four rounds.

Like the mass balance breakdown, the theoretical energy consumption breakdown is plotted in Fig. 12. The early rounds have a higher energy rate because the material weight is higher than the later rounds and because early rounds spend energy on processing large material weights. Notably, approximately 75% of the energy consumption in the four rounds (excluding the directional solidification process) is spent on aluminum heating, whereas the heat of Si fusion in Al plays a small role in reducing the total amount of power spent on heating the system. It was revealed that the heat of fusion adds around 23% of the required energy to heat the system at temperatures < 600 °C, but the contribution reduces to only 10% of the required energy at temperatures > 1000 °C.[48] The estimated energy rate (i.e., per 1 kg SoG-Si) is in the range of a single purification round.

The results of the energy evaluation are summarized in Table III. In summary, the theoretical evaluation of the energy consumption to purify Mg-Si to SoG-Si is depicted in Table III. The results reveal the importance of recycling the Al alloys resulting in the higher purity rounds of purification and reusing them in the lower purity rounds. The theoretical energy consumption can be reduced by around 19–28% when partly recycling Al, and the recovery rate can theoretically be improved up to 49–70% (based on the amount of recycled Al used in the purification). This is mainly because of the significant improvement of the Si recovery. The number of purification processes and the need to use recycled Al is mainly driven by the level of B in the raw material, i.e., the MG-Si. The higher the B concentration is, the less the need to use recycled Al alloy.

Table III. Summary of the evaluation of the energy consumption per mass unit of SoG-Si for the metallurgical purification method

	Without Al recycling (scenario 1)	Al alloy used for Round 1 (scenario 2)	Al alloy used for rounds 1 & 2 (scenario 3)	Al alloy used for rounds 1, 2, & 3 (scenario 4)
Si recovery	36.66%	40.82%	49.72%	70.10%
Energy rate (kWh/kg_{SoG-Si})	5.83	5.56	4.71	4.18
Primary Al used in the process (kg_{Al}/kg_{SoG-Si})	8.44	7.04	4.86	1.95
Recycled Al used in the process (kg_{Al}/kg_{SoG-Si})	0.0	1.39	3.17	5.11

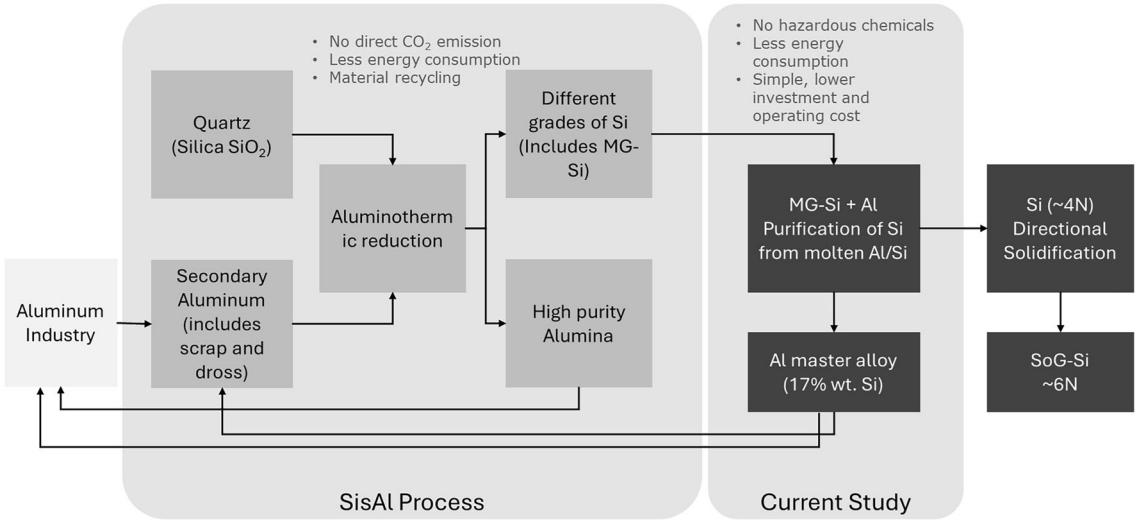

Fig. 13. Illustration of integration of metallurgical purification in Al-Si melt with the SisAl process.

There are two sources of Al: the first one is the recycled Al from previous processes, and the second source is the primary Al material that was introduced to the process. The energy required to produce the Al is not considered in this study since the resulting secondary product, the high-silicon Al alloy, has several applications in industry.

Al-Si alloy is distinguished by its good weldability, high thermal conductivity, and high specific strength at elevated temperatures. Additionally, it offers superior wear and corrosion resistance. Owing to these beneficial properties, Al-Si alloy is extensively employed in the aerospace, automotive, and military industries.[49]

Another option for using the master alloy will be possible once the SisAl process is commercialized by reusing the master alloy in the aluminothermic reduction of silicon (Fig. 13). This scenario offers strong integration of metallurgical purification in Al-Si melt with the SisAl pilot process and helps to form a circular economy for the silicon industry.

The practical assessment of the energy was reported by Silicor,[35] where the consumed energy ranges between 10 and 25 kWh/kg with a significant difference with the current situation for the electronic grade industry that requires 75–125 kWh/kg.

CONCLUSION

The SisAl Pilot project provides a novel method for producing MG-Si from SiO_2 by an aluminothermic process using a silica-rich slag and secondary aluminum from the ferroalloy and aluminum industries. Here, the purity of such MG-Si was increased by more than two orders of magnitude by dissolving it into an Al melt and then crystallizing it again by slow cooling. The process is promising for purifying

low-grade Si, towards SoG purity, with less environmental effect than current technology. The conclusion of the study:

- Dissolving MG-Si in molten Al and precipitating Si out of the melt effectively reduce the contamination of most impurities, including B and P with a final concentration of 314 ppb_a and 96 ppb_a, respectively, besides the high calcium content resulting from the SisAl process. This purity level permits further silicon refining by directional solidification to reach the solar-grade silicon.
- The purification process has a recovery rate of the Si ($\sim$ 49% to 70%), but there is a trade-off between the recovery rate and the purity level. More rounds of dissolution and precipitation increase the purity level but at the expense of the recovery rate which gets lower. Si recovery can be improved by recycling the Al used for higher-purity steps for the lower-purity steps. Furthermore, the unrecovered Si is not lost, because the spent melts can be used as a master alloy for making Al alloy products.
- Reusing the Al of the high-purity steps leads to a significant increase in the silicon recovery, which reduces the theoretical required energy to produce a mass unit of SoG-Si. The impact of recycling aluminum is tremendous when the energy required for primary aluminum is included in the assessment of the total energy of the solar silicon.

ACKNOWLEDGEMENTS

The authors gratefully acknowledge the SisAl Pilot project for funding this work (EU H2020 program, grant: 869268), Bochang Chen for his work with sample preparation and acid leaching, and Gísli Porsteinsson for technical support. The authors wish to thank the technical and administrative staff of Reykjavik University, Elkem, Hydro, Silicor Materials, and all SisAl Pilot project's partners for their assistance during this work.

CONFLICT OF INTEREST

On behalf of all authors, the corresponding author states that there is no conflict of interest.

OPEN ACCESS

REFERENCES

1. E. Kabir, P. Kumar, S. Kumar, A.A. Adelodun, and K.H. Kim, *Renew. Sustain. Energy Rev.* 82, 894 https://doi.org/10.1016/j.rser.2017.09.094 (2018).
2. D.M. Danielsson, J.T. Gudmundsson, and H.G. Svavarsson, *Phys. Scr.* T141, 014005 https://doi.org/10.1088/0031-8949/2010/T141/014005 (2010).
3. D. Yan, *in Handbook of Photovoltaic Silicon* (Springer, Berlin, Heidelberg, 2020), pp1–31.
4. G. Sævarsdottir, H. Kvande, and T. Magnusson, Proc. 16th Int. Ferro-Alloys Congr. (INFACON XVI) (2021). https://doi.org/10.2139/ssrn.3926088.
5. L. Stamford and A. Azapagic, *Energy Technol.* 6, 1148 https://doi.org/10.1002/ente.201800037 (2018).
6. J.O. Odden, G. Halvorsen, H. Rong, and R. Gløckner, in Silicon for the Chemical and Solar Industry IX (2008), pp. 75–90.
7. M.D. Johnston, L.T. Khajavi, M. Li, S. Sokhanvaran, and M. Barati, *JOM* 64, 935 https://doi.org/10.1007/s11837-012-0384-3 (2012).
8. X. Ma, J. Zhang, T. Wang, and T. Li, *Rare Met.* 28, 221 https://doi.org/10.1007/s12598-009-0043-1 (2009).
9. F. Chigondo, *SILICON* 10, 789 https://doi.org/10.1007/s12633-016-9532-7 (2018).
10. M. Heuer, in Semiconductors and Semimetals, ed. G.P. Willeke and E.R. Weber (Elsevier, 2013), Vol. 89, pp. 77–134. https://doi.org/10.1016/B978-0-12-381343-5.00002-1.
11. T. Yoshikawa and K. Morita, *J. Cryst. Growth* 311, 776 https://doi.org/10.1016/j.jcrysgro.2008.09.095 (2009).
12. Y. He, W. Ma, A. Xing, M. Hu, S. Liu, X. Yang, J. Li, S. Du, and W. Zhou, *Mater. Sci. Semicond. Process.* 141, 106438 https://doi.org/10.1016/j.mssp.2021.106438 (2022).
13. E. Olsen and S. Rolseth, *Metall. Mater. Trans. B* 41, 295 https://doi.org/10.1007/s11663-010-9362-8 (2010).
14. M. Tao, *Electrochim. Acta* 89, 688 https://doi.org/10.1016/j.electacta.2012.10.148 (2013).
15. K. Yasuda and T. Nohira, *High Temp. Mater. Processes* 41, 247 https://doi.org/10.1515/htmp-2022-0033 (2022).
16. H.M. Liaw and F. Secco d'Aragona, Sol. Cells, 10, 109 (1983). https://doi.org/10.1016/0379-6787(83)90012-1.
17. L.A.V. Teixeira, and K. Morita, *ISIJ Int.* 49, 783 https://doi.org/10.2355/isijinternational.49.783 (2009).
18. M. Johnston and M. Barati, *Sol. Energy Mater. Sol. Cells* 94, 2085 https://doi.org/10.1016/j.solmat.2010.06.025 (2010).
19. H. Bjerke, Removal of Boron from Silicon by Slag Treatment and by Evaporation of Boron from Slag in Hydrogen Atmosphere (Master's Thesis, Institutt for Materialteknologi, 2012).
20. Z. Ding, W. Ma, K. Wei, J. Wu, Y. Zhou, K. Xie, and J. Non-Cryst, *Solids* 358, 2708 https://doi.org/10.1016/j.jnoncrysol.2012.06.031 (2012).
21. J.F. White and D. Sichen, *Metall. Mater. Trans. B* 45, 96 https://doi.org/10.1007/s11663-013-0010-y (2014).
22. J. Safarian, G. Tranell, and M. Tangstad, *Energy Procedia* 20, 88 https://doi.org/10.1016/j.egypro.2012.03.011 (2012).
23. J. Safarian and M. Tangstad, *Metall. Mater. Trans. B* 43, 1427 https://doi.org/10.1007/s11663-012-9728-1 (2012).
24. A. Hoseinpur, G. Tranell, and J. Safarian, in Silicon for the Chemical and Solar Industry XV (2020), p. 261.
25. A. Hoseinpur, S. Andersson, K. Tang, and J. Safarian, *Langmuir* 37, 7473 https://doi.org/10.1021/acs.langmuir.1c00876 (2021).

26. Y. Ren and K. Morita, *ACS Sustain. Chem. Eng.* 8, 6853 https://doi.org/10.1021/acssuschemeng.0c01785 (2020).
27. M.D. Johnston and M. Barati, *Sep. Purif. Technol.* 107, 129 https://doi.org/10.1016/j.seppur.2013.01.028 (2013).
28. X. Ma, T. Yoshikawa, and K. Morita, *J. Cryst. Growth* 377, 192 https://doi.org/10.1016/j.jcrysgro.2013.05.024 (2013).
29. M. Heuer, M. Kaes, T. Bartel, A. Turenne, and T. Jester, *Silicon for the Chemical and Solar Industry XIII* (Trondheim, Norway, 2016).
30. E. Forniés, L. Méndez, and M. Tojeiro, *Photovolt. Int.* 31, 29 (2016).
31. H. Chen, K. Morita, X. Ma, Z. Chen, and Y. Wang, *Sol. Energy Mater. Sol. Cells* 203, 110169 https://doi.org/10.1016/j.solmat.2019.110169 (2019).
32. T. Yoshikawa and K. Morita, *Metall. Mater. Trans. B* 36, 837 https://doi.org/10.1007/s11663-005-0076-2 (2005).
33. T. Yoshikawa, K. Arimura, and K. Morita, *Metall. Mater. Trans. B* 36, 837 https://doi.org/10.1007/s11663-005-0085-1 (2005).
34. R.K. Dawless, R.L. Troup, D.L. Meier, and A. Rohatgi, *J. Cryst. Growth* 89, 68 https://doi.org/10.1016/0022-0248(88)90073-5 (1988).
35. T. Jester, *Renew. Energy Focus* 15, 34 https://doi.org/10.1016/S1755-0084(14)70045-6 (2014).
36. K. Morita and T. Yoshikawa, *Trans. Nonferrous Met. Soc. China* 21, 685 https://doi.org/10.1016/S1003-6326(11)60766-8 (2011).
37. J.W. Li, Z.C. Guo, H.Q. Tang, and J.C. Li, *High Temp. Mater. Processes* 32, 503 https://doi.org/10.1515/htmp-2012-0157 (2013).
38. M.A. Martorano, J.B. Ferreira Neto, T.S. Oliveira and T.O. Tsubaki, Mater. Sci. Eng. B, 176, 217 (2011). https://doi.org/10.1016/j.mseb.2010.11.010.
39. H. Philipson, G.L. Solbakk, M. Wallin, K.E. Einarsrud, and G. Tranell, in Light Metals 2022 (Springer, Cham, 2022), pp. 1038–1045. https://doi.org/10.1007/978-3-030-92529-1_135.
40. H. Philipson, M. Wallin, K.E. Einarsrud, and G. Tranell, in Proc. 16th Int. Ferro-Alloys Congr. (INFACON XVI) (September 2021).
41. A. Toli, G.M. Tsaousi, E. Balomenos, D. Panias, M. Heuer, H. Philipson, and G. Tranell, *Mater. Proc.* 5, 85 https://doi.org/10.3390/materproc2021005085 (2021).
42. J.L. Murray and A.J. McAlister, *Bull. Alloy Phase Diagrams* 5, 74 https://doi.org/10.1007/BF02868729 (1984).
43. E. Scheil, *Int. J. Mater. Res.* 34, 70 https://doi.org/10.1515/ijmr-1942-340303 (1942).
44. R.A. Brown and D.H. Kim, *J. Cryst. Growth* 109, 50 https://doi.org/10.1016/0022-0248(91)90157-Z (1991).
45. I.C. Santos, A.P. Goncalves, C.S. Santos, M. Almeida, M.H. Afonso, and M.J. Cruz, *Hydrometallurgy* 23, 237 https://doi.org/10.1016/0304-386X(90)90007-O (1990).
46. Y. Delannoy, M. Heuer, E. Øvrelid, and S. Pizzini, in Solar Silicon Processes: Technologies, Challenges, and Opportunities (CRC Press, 2017), p. 83.
47. J. Safarian, L. Kolbeinsen, and M. Tangstad, *Metall. Mater. Trans. B* 42, 852 https://doi.org/10.1007/s11663-011-9507-4 (2011).
48. A.R. Mallah, H.G. Svavarsson, M. Heuer, and G. Sævarsdottir, *Proc. Silicon Chem. Sol. Ind.* 17, 1 https://doi.org/10.2139/ssrn.4942485 (2024).
49. J. Park, I. Yeo, I. Jang, and S. Jeong, *J. Mater. Process. Technol.* 266, 283 https://doi.org/10.1016/j.jmatprotec.2018.11.007 (2019).